Ammonia Sensing using Arrays of Silicon Nanowires and Graphene

K. Fobelets[1†], C. Panteli[1], O. Sydoruk[1], C.B. Li[2]
[1]OSD, Electrical and Electronic Engineering Department, Imperial College London, Exhibition Road, SW7 2BT London, UK
[2]Institute of Semiconductors, Chinese Academy of Sciences, Beijing 100083, China

Abstract: Ammonia (NH_3) is a toxic gas released in different industrial, agricultural and natural processes. It is also a biomarker for some diseases. These require NH_3 sensors for health and safety reasons. To boost the sensitivity of solid-state sensors, the effective sensing area should be increased. Two methods are explored and compared using an evaporating pool of 0.5 ml NH_4OH (28% NH_3). In the first method an array of Si nanowires (Si NWA) is obtained via metal-assisted-electrochemical etching to increase the effective surface area. In the second method CVD graphene is suspended on top of the Si nanowires to act as a sensing layer. Both the effective surface area as well as the density of surface traps influences the amplitude of the response. The effective surface area of Si NWAs is 100x larger than that of suspended graphene for the same top surface area, leading to a larger response in amplitude by a factor of ~7 notwithstanding a higher trap density in suspended graphene. The use of Si NWAs increases the response rate for both Si NWAs as well as the suspended graphene due to more effective NH_3 diffusion processes.

Key words: NH_3 sensor; silicon nanowires; resistive sensor; low frequency noise, graphene
PACS: 07.07.Df; 73.50.Td **EEACC:** 2140; 2560R

1. Introduction

Ammonia (NH_3) is a noxious gas that can be lethal at high concentrations or long exposure times. It is both produced by natural processes such as decomposition of biological materials as well as by the manufacturing industry such as in e.g. industrial refrigeration [1]. Although the human nose can detect NH_3 odor at a low non-hazardous level of 5-10 ppm [2], detectors are still needed for health and safety and also for medical diagnostics. Detectors in the industrial application domain do not need to be fast nor have ultrahigh sensitivity, the 8 hr time-weighted average exposure limit is approximately 25 ppm. However, medical diagnostics such as the use of NH_3 as a biomarker for liver and kidney disease [3] requires highly sensitive, selective and compact devices. Current research investigates non-invasive measurement techniques such as e.g. breath analysis for the detection of NH_3. In this case, the sensor detection limit needs to go down to ~ 50 ppb. In all these cases interfering gases will be present including H_2O, CO, NO_x… Sensors thus need selectivity in order to distinguish between the different gases within a mixture.

Different types of sensing methods exist, including electrochemical, electrical (e.g. resistive, capacitive, amperometric …), optical (e.g. surface plasma resonance) and mechanical (piezo-electric) [4,5]. Solid-state electrical sensors come with the benefits of recovering to their original state due to the gas adsorption/desorption process; CMOS integration possibilities for readout and control; and compactness. However, their sensitivity to the background gases mentioned above is problematic. Approaches to improve the selectivity of the sensors are based on functionalization with selective layers, often consisting of nanoparticles [6]. Since the adsorption of gases on the sensing surface influences its character, another method to improve selectivity is to probe the electrical characteristics of the surface via low frequency noise measurements [7]. Since NH_3 is an electron

http://www.pdf-tools.com

donor, its presence changes not only the electrical conductivity of the sensor but can also influence the low frequency noise of the sensor via interaction with surface traps [8]. The combination of conductivity change and change in low frequency noise characteristics can be exploited to increase the selectivity of the sensor and is also a tool to better understand the processes occurring at the surface of the sensors.

In order to increase the sensitivity of the resistive-based solid-state sensors, the effective surface area can be increased and/or the dimensions of the sensing channel can be reduced to increase the surface to volume ratio. 1-dimensional structures are of particular interest for this purpose [9]. Their fabrication and operation are schematically illustrated in Table 1.

Table 1: Different configurations of nanowire/rod based sensors with their particular characteristics [10].

Nano-wires/-rods	**Structure**	**Response time**	**Effective Detection Surface**	**Carrier Transport Mechanism**	**Fabrication**
Single		Fast (~10 s)	Small	1D	Complex
Aligned array		Slow (order of minutes)	Large	1D	Complex/easy
Random distribution		Slow (order of minutes)	Large	Hopping	Easy

A wide range of top down and bottom up methods exist to fabricate 1D structures. Amongst the bottom up techniques low and high temperature CVD, MBE, laser ablation, and others can be found [11]. Characteristics of these approaches are versatility, good control over morphology, large material diversity, very small diameter, but also kinks in growth direction, difficulty to control doping and catalyst related defects.

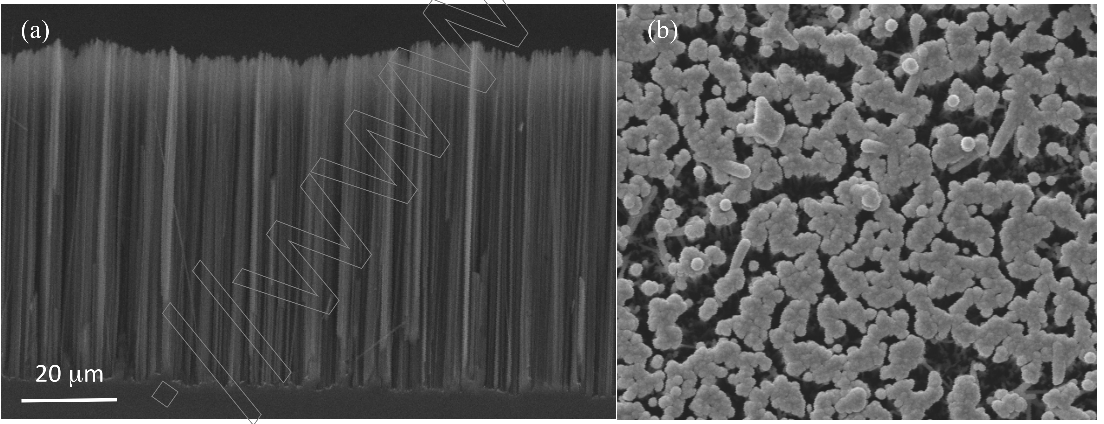

Figure 1: SEM of (a) side view of a MACE etched Si nanowire array and (b) top view after metallisation.

Lithography and etching can be used as top down techniques. A top down approach that does not require lithography is based on metal-assisted chemical etching (MACE) which is a wet chemical process in “ambient” in which noble metal particles (Ag, Au, Pt, …) on the surface act as catalyst for H^+ generation to locally oxidise the semiconductor. For Si-based materials HF then dissolves the

http://www.pdf-tools.com

SiO_2, generating directional pits [12,13]. This gives a random array of nanowires with a diameter range of 50 nm < d < 300 nm and a length determined by the etch times and ambient conditions. Template based MACE increases the number of required process steps but leads to better control and uniformity of the nanowire diameter [14]. The main characteristics of the MACE process are its simplicity, low cost, easy process control and doping determined by the substrate. However, the etch is strongly doping concentration dependant, the material choice is limited and the process is wasteful in material use.

In this manuscript MACE will be used to fabricate Si nanowire arrays (Si NWAs) for the sensors. A SEM micrograph of a typical Si NWA used in this work is given in figure 1, showing a parallel connection of well-aligned nanowires attached to the Si substrate. Evaporation of a metal contact under an angle with respect to the nanowires, leaves top access for gas ad-/desorption.

In addition to a wide range of semiconducting nanostructures used for gas sensing, graphene has also become a popular material for sensing purposes, driven by its 2D character, chemical stability and high electrical conductivity [15]. In particular, CVD graphene has been studied widely because of its potential for upscaling to commercial applications [16]. As with other solid-state sensors, also graphene is sensitive to multiple gases. Selectivity can be obtained between gases donating a different carrier type such as NH_3 (electron donor) and NO_2 (electron acceptor). However in many practical sensing applications H_2O (in the form of relative humidity) will be present and influences the response of the sensors. It has been demonstrated that low frequency noise characterization of graphene and its response to different gases might help improve selectivity without the need for surface functionalization. In [17] selectivity was obtained between solvents via the different shift of the lifetime of the generation-recombination center determined in the low frequency noise characteristics. Although, graphene offers a large surface to volume ratio, only half of the surface is available for easy molecule adsorption as the graphene layer needs to be supported onto a substrate.

In this manuscript we report on the combination of graphene and Si NWAs. Graphene is transferred onto the NWA making the bottom area of the graphene available for molecule adsorption. The combination of Si NWAs and graphene leads to higher improvements in sensitivity of the graphene layers than when graphene resides on a solid surface. A SEM micrograph of a graphene layer on a Si NWA is given in figure 2. The Si NWs in this figure are bundled at the top due to capillary effects in the wet chemical process and Van der Waals forces.

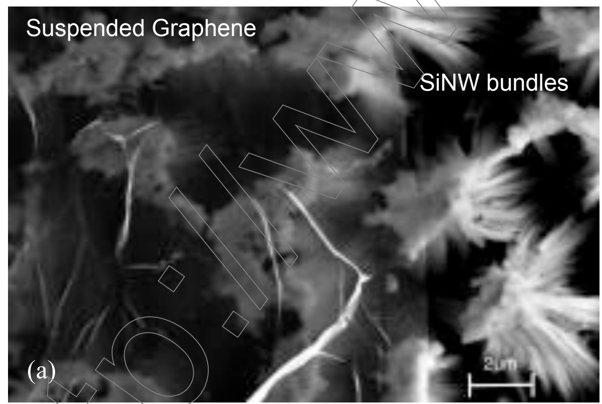

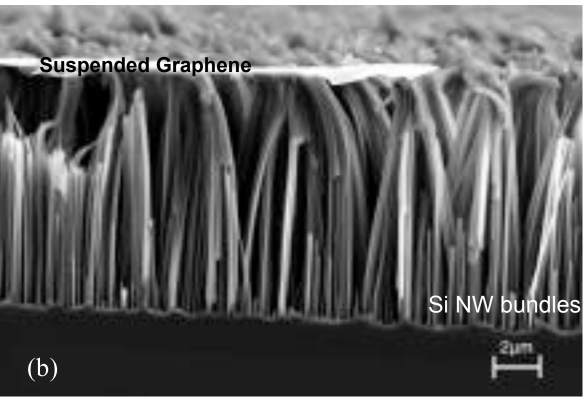

Figure 2: SEM images. (a) Top view of a graphene layer covering 2/3rd of the Si NWA in the image. Graphene can be seen as a milky shine on top of the Si NWA. (b) Side view of the suspended graphene layer that can be seen as a white sheet on top of the Si NWA.

http://www.paper.edu.cn

In this manuscript we will qualitatively compare the resistive and electrical low frequency noise response of Si NWAs and graphene supported by Si NWAs.

2. Experiment

2.1 Sample preparation

The Si NWAs are fabricated using MACE on (100) substrates. For the Si NWA sensors, Si samples of ~1 cm × 1 cm with a resistivity, ρ = 1-10 Ω cm were used. Work is carried out on p- (acceptor doped using B atoms) as well as n-type (donor doped using As atoms) Si. One surface of the sample is protected with a poly methyl methacrylate (PMMA) layer during etching. After cleaning, the sample is immersed in a solution of 0.03 M $AgNO_3$: 5.6 M HF for 3 hrs. This one-step MACE process creates vertically aligned Si NWs attached to the remaining Si substrate (see figure 1). The residual Ag particles, left during the MACE process, are removed using a concentrated (5 M) solution of HNO_3. Finally, the PMMA layer is removed in acetone. Ohmic contacts are defined on *p*-type Si NWAs using a sputtered ~50/500 nm Cr/Au, and on *n*-type using ~500 nm Al. Different metals are used to ensure Ohmic contact behavior for the two doping types. The native oxide is removed prior to metallization in a 4% HF solution for 2 min. Rapid thermal annealing in Ar ambient at 450°C is used to improve the contact characteristics.

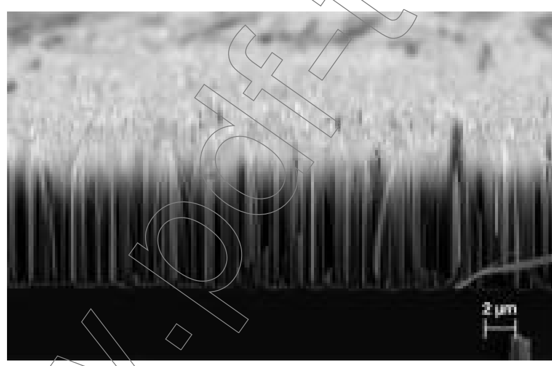

Figure 3: SEM of the nanowire array used for suspended graphene sensing using 4 ml $AgNO_3$.

For the suspended graphene layer, the Si NWA was etched in a two-step MACE process. A clean ~1 cm × 1 cm (100) p-Si sample was used with ρ = 1-5 Ω cm. In the first step the sample was immersed in 4 ml $AgNO_3$: 4 ml of 50% HF : 12 ml H_2O for 10 min at room temperature. This nucleates Ag nanoparticles (NPs) on the surface. After rinse the sample is then immersed in 10 ml H_2O_2 : 4 ml 50% HF : 6 ml H_2O for 10 min. The Ag NPs act as catalyst for the oxidation and etch process, leaving behind vertically aligned NWs (see figure 2). The relatively high volume of 4 ml $AgNO_3$ was used for the graphene experiments to deliver sharp unbundled NWs [18] (see figure 3) unlike in figure 2 where the $AgNO_3$ volume was half, 2 ml. Using a higher concentration of $AgNO_3$ in the mixture results in shorter NWs, however the unbundled NWs allows more access to the graphene back surface [19]. The difference in the Si NWA geometry caused by one-step and two-step MACE [20] has no impact on the results as the role of the NWA is as passive support only in the graphene sensor. Multilayer (3 – 8 layers) CVD graphene on Ni was used for the suspended graphene experiments. The recipe for the graphene transfer process uses a PMMA supporting layer as reported in [21,22]. Ni is etched in 3 HPO_4 : 3 HNO_3 : 1 CH_3COOH : 1 H_2O. The detached graphene is then

http://www.pdf-tools.com

transferred onto the Si NWA. Finally, the PMMA layer is dissolved in acetone vapor at 86 °C for 1 hr, resulting in a very strong bond between the graphene and the Si NWA. The same process was applied to transfer graphene onto a clean SiO_2 control sample.

2.2 Measurement set-up

Electrical measurements are performed using an Agilent 4155B or Keysight B1500A semiconductor device analyzer. The Si NWA sensors are biased at constant voltage and the current is measured as a function of time in steps of 4 s. For the graphene-based sensors, a constant current of 50 µA was supplied and the voltage variation was measured as a function of time. The schematic of the experimental set-up can be found in figure 4a. NH_4OH (28 wt% NH_3 in H_2O) is introduced into the measuring chamber using a 3.5 cm high cylindrical beaker with a diameter of 3.5 cm and positioned ~1 cm from the sensor. Due to the low concentration of NH_4OH, the dissociation process follows mainly $NH_4OH \leftrightarrow NH_3 + H_2O$. The mass transfer factor of NH_3 is, $k \approx 0.32\ 10^{-2}$ m/s for very low wind speed, thus NH_3 evaporates readily from the NH_4OH pool and will arrive within ~6 s at the surface of the sensor [23,24]. It was found that a 0.5 ml pool of NH_4OH was sufficient to saturate the Si NWA samples. The electrical measurements on the Si NWAs are carried out by contacting the NWs with a flat spring-loaded probe tip of 3 mm diameter and a back contact via the Cu back plate. For the graphene measurements, two of the four 3 mm diameter spring-loaded probes are used in a horizontal configuration, separated by ~3 mm and aligned vertically. All probes are Au coated to avoid corrosion.

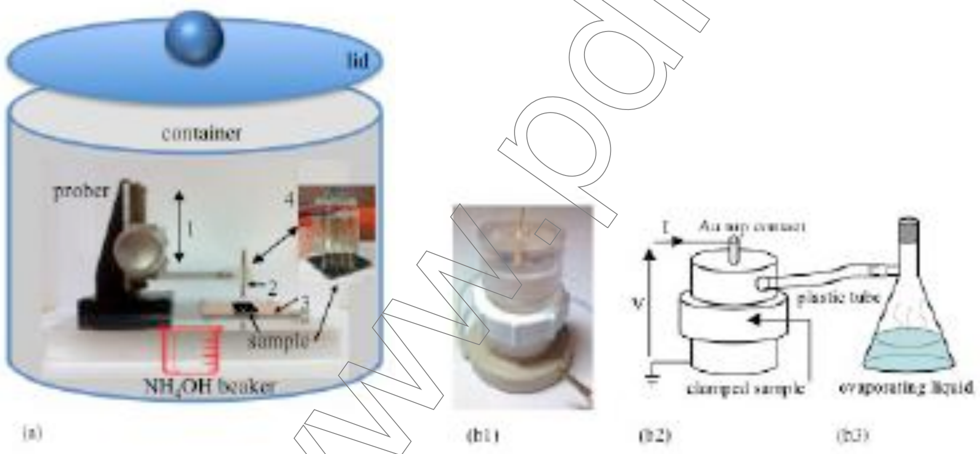

Figure 4: (a) the measurement set-up for resistance measurements. 1: z-axis translation, 2: flat spring loaded probe tip for Si NWA measurements, 3: back plate for back contact, 4: 4 parallel, equidistant (3 mm) probe tips for graphene measurements. Probe configuration 2 and 4 can be interchanged. All probe tips are Au coated and have a diameter of 3 mm. (b1) Closed container and schematic set-up ((b2) container, (b3) conical flask attached to container) used for low frequency noise measurements on Si NWA.

The low-frequency noise measurements use a dedicated closed cylindrical container with a volume of $V \approx 1.6$ cm^3 (see figure 4b). The sample was saturated with evaporating NH_3 before measurements. The container was placed in an E-M shield and the devices biased using a battery. Contacts were made with a 3 mm diameter Au top probe under controlled pressure onto the NWA and a Cu back plate. Noise data was obtained in a frequency range from 1 Hz to 1 kHz at 300 K for the NWA under

http://www.pdf-tools.com

constant bias. Background noise was measured using the zero-biased set-up and subtracted from the total device noise. The voltage fluctuations S_V from the load resistor R_L connected in series with the NWA were analyzed using a SR770 FFT Spectrum Analyzer. The spectral noise density of the short circuit current fluctuations, S_I, was calculated using the expression:

$$S_I = S_V \left[\frac{R_L+R_d}{R_L \times R_d}\right]^2$$

where R_d is the sensor's differential resistance.

3. Results and discussion

3.1 Measurements on Si NWAs

To measure the response to evaporating NH_3, the beaker with 0.5 ml NH_4OH was placed in the container and the lid was closed [25,26,27,28]. For the desorption process the lid and the NH_4OH recipient were removed from the container. Since the different sensors have different initial resistance values, the resistance change is normalized to the resistance value in air. Figure 5a) shows the measured adsorption/desorption characteristics on the p-Si NWA. The adsorption characteristic of NH_3 is repeated in figure 6a) (dashed line).

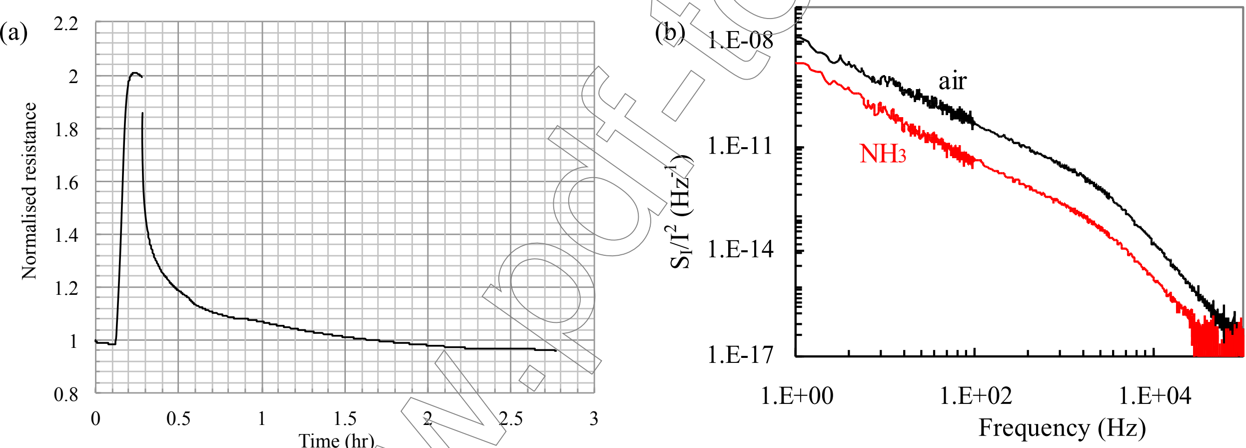

Figure 5. (Color online) (a) The measured normalized resistance variation as a function of time for the adsorption/desorption process on p-Si NWA. (b) The normalized low frequency current noise spectra with and without NH_3 (both axes are on log scale).

NH_3 is introduced at t = 0.12 hr, the resistance changes immediately and full saturation of the characteristics is reached within 0.08 hr (4.8 min). The normalized resistance changes by a factor of 2. The increase in resistance confirms the electron donor characteristics of NH_3. The same measurement on n-Si NWA is shown in figure 6a) (full line). The normalized resistance change is a factor of ~10, whilst the time to full saturation is approximately half of that of the p-type sample. The improved response of the n-type wires is due to longer NWs in the array for n-type wires compared to p-type wires for the same etch recipe as described in [12]. A second factor that plays a role in the response is the thickness of the native oxide surrounding the NWs and the diameter of the wires. These parameters are strongly influenced by the doping type and density of the original Si wafer. The response of the n-Si NWA is opposite to that of the p-Si NWA, as expected. The electron donating character of NH_3 depletes the p-Si surface whilst it accumulates electrons at the n-Si

http://www.pdf-tools.com

surface. The desorption shows a "fast" and slow response time. Initially, desorption and adsorption are at approximately the same rate. However, in order to fully recover, all NH_3 molecules need to be removed from the NWA which takes ~2 hrs. The NWA traps the NH_3 molecules between the NWs slowing the desorption process. Heating of the NWA can improve the desorption rate. The low frequency noise measurements for p and n-Si NWA are given in figure 5b) and 6b), respectively [29,30,31]. Interestingly, the variation of the low frequency noise for both samples are in the same direction because NH_3 passivates the electron traps in the oxide that surrounds the NWs, resulting in a decrease in carrier number fluctuations in the Si NW conducting channel and thus decreases the low frequency noise. The relevance of this is for selectivity as other gases with a different influence on the oxide traps related to the MACE process might cause similar resistance changes but different variations of the electrical noise [8,10]. In figure 5b) a generation-recombination (GR) shoulder appears in the low frequency noise plot at ~1 kHz. This specific GR trap is not influenced by the gas adsorption because the trap does not occur in the oxide layer but is associated to a bulk-related trap in the NWs.

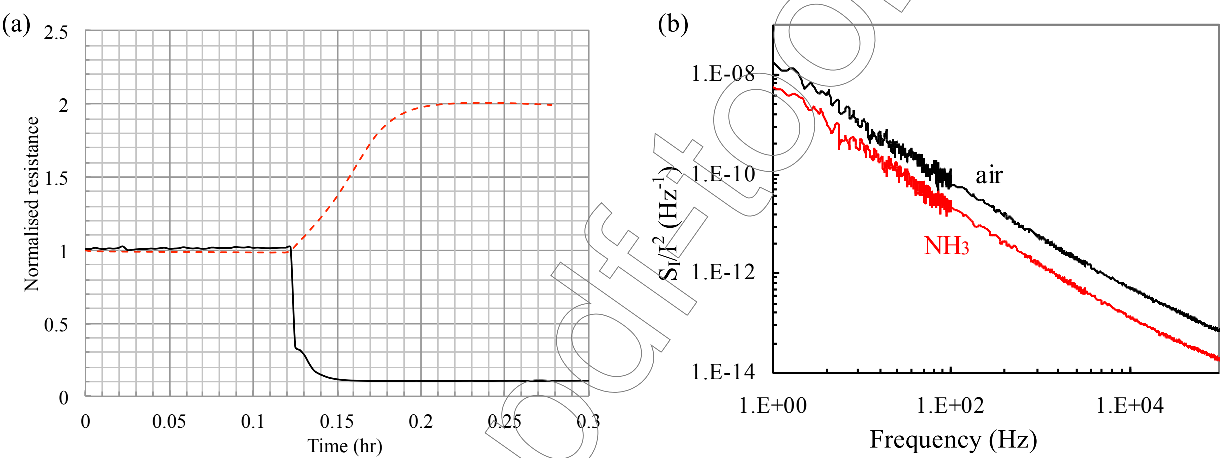

Figure 6. (Color online) (a) The measured normalized resistance variation as a function of time for the adsorption process on n-Si NWA (full line) and p-Si NWA (dashed line). (b) The normalized low frequency current noise spectra with and without NH_3 (both axis are on log scale).

3.2 Measurements on suspended graphene

The measurements on suspended graphene on a Si NWA and graphene-on-oxide were carried out in a 2-horizontal probe configuration. The graphene surface area is approximately 1 cm^2, similar to the NWA area in the previous measurements. In figure 7 the normalized resistance is plotted as a function of time for both suspended graphene on a Si NWA and graphene on SiO_2.

The relative resistance increases in both systems, similar to the response of the p-Si NWA, implying that the graphene layer is p-type. Comparing the response of suspended graphene to graphene on SiO_2 shows some interesting features: the initial response rate (variation of 10% from the initial value) of suspended graphene is ~10 times faster than graphene on SiO_2. Similarly the desorption rate of suspended graphene is ~20 times higher than that of graphene on SiO_2. Although none of the sensors have saturated within 1 hr 45 min, the amplitude of the normalized resistance of suspended graphene is 1.2× higher within the same timeframe. The difference in behavior is caused by both the increase in effective surface area of suspended graphene compared to graphene on SiO_2 – since the

bottom graphene surface has become available for adsorption – as well as the different diffusion dynamics of the NH_3 molecules in the two systems. When NH_3 molecules reach the sensors, some will adsorb on the top surface whilst others will diffuse through the system before adsorption. Since the suspended graphene allows more room for this diffusion process through the gaps between the nanowires its rate is higher, both in the adsorption as well as the desorption process.

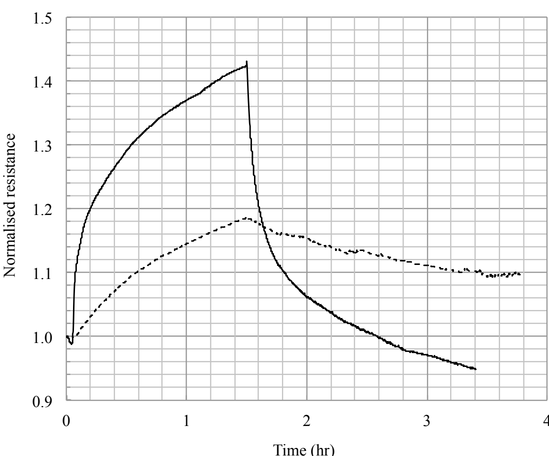

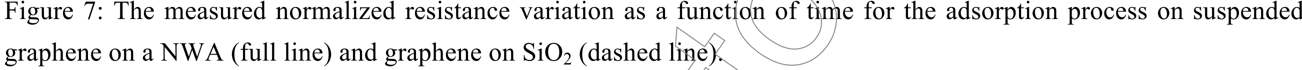
Figure 7: The measured normalized resistance variation as a function of time for the adsorption process on suspended graphene on a NWA (full line) and graphene on SiO_2 (dashed line).

Comparing the time to saturation of the suspended graphene system to the nanowire-only system shows that the response rate of the NWA-only system is at least 5× higher than the graphene system, indicating slower adsorption dynamics on graphene. Similarly, the amplitude of the resistance variation with the same pool of NH_4OH is much higher for the NWA-only sample. This feature is related to the number of available adsorption sites in the system influenced by the effective surface area but also by the uncompleted bond density at the surface that allows adsorption of NH_3. Since the density of NWs is approx. 10^9 cm^2 and taking an average NW diameter of 250 nm, the effective surface area of the 60 μm long Si NWA is A_{NWA} ≈ 3 10^3 mm^2. This is much larger than that of suspended graphene with A_{susGr} ≈ 20 mm^2 (determined approximately by the distance between the probes and the probe diameter).
The influence of the surface states can be analysed via low frequency noise measurements. The normalized low frequency current noise power spectral density for the graphene systems is given in figure 8. The low frequency noise spectral density of the graphene system is proportional to I^2. This implies that the electrical current I does not drive the fluctuations but merely makes the fluctuations in the sample visible if Ohm's law is used [32]. This is what is usually observed for graphene where noise is related to carrier number and/or mobility variations, similar to the Si NWA system. The amplitude of the normalised noise spectral density measured in our system is also within that reported for graphene: 10^{-7} – 10^{-9} Hz^{-1} at 10 Hz [24]. In our system, no specific G-R centres are observed in the samples in contrast to [17]. In consequence, the noise measurements in this case cannot identify directly the molecule type adsorbed. From figure 8 we can observe that the noise spectra follow a 1/f characteristic and that in the presence of NH_3 molecules, the noise is reduced. This behaviour is identical to that on Si NWA proving that NH_3 passivates the surface traps in the graphene system. Another observation is the higher amplitude of the normalised noise in the suspended graphene layer. This is consistent with the hypothesis that the amplitude of the response to

http://www.pdf-tools.com

NH_3 is driven by the surface condition of the sensor. The amplitude response of the suspended graphene is indeed larger than that of graphene on oxide.

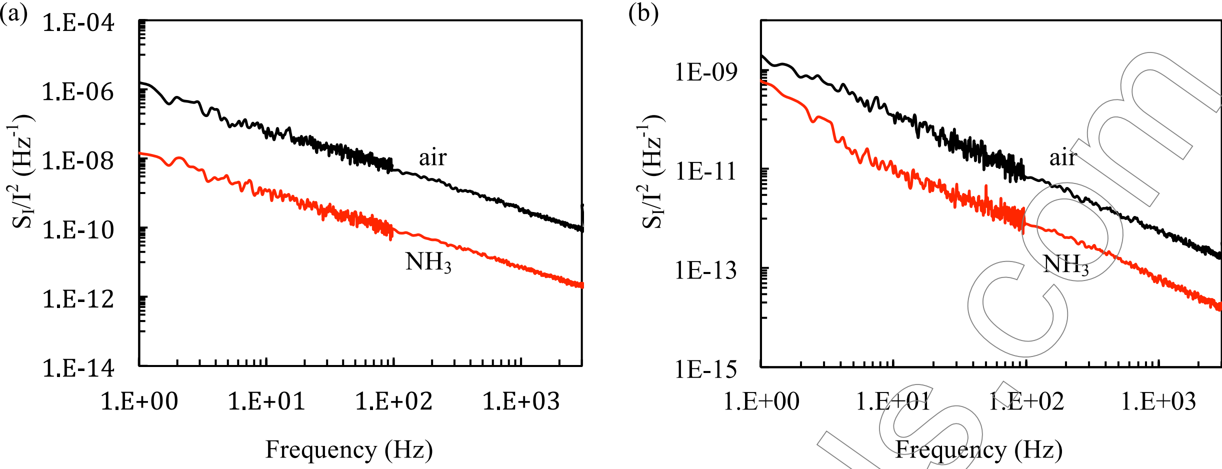

Figure 8: The normalized low frequency current noise spectra with and without NH_3. (a) Suspended graphene on Si NWA. (b) Graphene on SiO_2 (both axes are on log scale).

4. Conclusion

The response of an n- and p-type Si NWA to NH_3 evaporating from a pool of 0.5 ml NH_4OH at room temperature is compared to the response of graphene suspended on a Si NWA and graphene on SiO_2. The response is given in terms of variations of the normalized resistance as a function of time and the normalized low frequency current noise spectral density with and without the presence of NH_3. It is found that the response is dependent on both the effective surface area as well as on the density of surface traps. The Si NWA systems offer an easy route towards increasing the effective surface area and as a consequence the variation of the normalized resistance upon admission of NH_3 is larger than for the graphene system with a similar top surface area. The response rate is strongly dependent on the diffusion of NH_3 through the sensor system. It is observed that the response rate on Si NWAs is faster than suspended graphene that in turn is faster than graphene on SiO_2. This is because NH_3 can more easily diffuse through a NW system. The noise spectra show the relationship between the density of surface traps and the response of the sensor. Although the density of surface traps is larger in suspended graphene than in the Si NWA, the much larger effective surface area of the Si NWA causes a larger amplitude response. However, comparing suspended graphene to graphene on SiO_2 it is observed that due to the larger trap density in suspended graphene and larger effective surface area its amplitude response is larger than that of graphene on SiO_2.

Acknowledgment

CP acknowledges financial support of EPSRC via the EEE department. C.L. and K.F. acknowledge support from e-on for the Si NWA sensing work.

http://www.pdf-tools.com

References

[1] B. Timmer, W. Olthuis, and A. van den Berg, “Ammonia sensors and their applications—a review”, Sensors and actuators B: Chemical 107(2), pp. 666-677 (2005).
[2] “IRC Ammonia sensor overview”, Industrial regfrigeration consortium, Dec. 2 2002. On-line: https://www.irc.wisc.edu/file.php?ID=44
[3] N. T. Brannelly, J. P. Hamilton-Shield and A. J. Killard, “The Measurement of Ammonia in Human Breath and its Potential in Clinical Diagnostics”, Critical Reviews in Analytical Chemistry 46(6), pp. 490-501 (2016).
[4] S. Lakkis, R. Younes, Y. Alayli, and M. Sawan, “Review of recent trends in gas sensing technologies and their miniaturization potential”, Sensor Review, 34(1) 24-35 (2014).
[5] G. Neri, “First Fifty Years of Chemoresistive Gas Sensors”, Chemosensors 3, 1-20 (2015).
[6] G. Korotcenkov, V. Brinzari, and B.K. Cho, “Conductometric gas sensors based on metal oxides modified with gold nanoparticles: a review”, Microchim Acta 183, pp. 1033-1054 (2016).
[7] J. M. Smulko, M. Trawka, C. G. Granqvist, R. Ionescu, F. Annanouch, E. Llobet, and L. B. Kish, "New approaches for improving selectivity and sensitivity of resistive gas sensors: a review", Sensor Review, 35(4), pp. 340-347 (2015).
[8] K. Fobelets, M. Meghani ans C. Li, “Influence of Minority Carrier Gas Donors on Low Frequency Noise in Silicon Nanowires”, IEEE Trans. Nanotechnol. 13(6), 1176-1180 (2014).
[9] M. M. Arafat, B. Dinan, Sheikh A. Akbar and A. S. M. A. Haseeb, “Gas Sensors Based on One Dimensional Nanostructured Metal-Oxides: A Review”, Sensors 12, pp 7207-7258 (2012).
[10] K. Fobelets, “Conductivity and 1/f noise in Si nanowire arrays”, E-MRS fall meeting, Warsaw (Poland), 15-18 Sept. (2015) (invited).
[11] V. Schmidt, J.V. Wittemann and U. Gösele, “Growth, Thermodynamics, and Electrical Properties of Silicon Nanowires”, Chem. Rev. 110, pp. 361–388 (2010).
[12] Z. Huang, N. Geyer, P. Werner, J. de Boor, and Ulrich Gösele, “Metal-Assisted Chemical Etching of Silicon: A Review”, Adv. Mater. 23, pp. 285–308 (2011).
[13] C. Li, K. Fobelets, C. Liu, C. Xue, B. Cheng, and Q. Wang, “Ag-assisted lateral etching of Si nanowires and its application to nanowire transfer”, Applied Phys. Lett. 103, 183102 (2013).
[14] Z. P. Huang, H. Fang, and J. Zhu “Fabrication of Silicon Nanowire Arrays with Controlled Diameter, Length, and Density”, Adv. Mater. 19(5), pp. 744–748 (2007).
[15] T. Wang, D. Huang, Z. Yang, S. Xu, G. He, X. Li, N. Hu, G. Yin, D. He, and L. Zhang, “A Review on Graphene-Based Gas/Vapor Sensors with Unique Properties and Potential Applications”, Nano-Micro Lett. 8(2), pp. 95–119 (2016)
[16] F. Yavari, E. Castillo, H. Gullapalli, P. M. Ajayan, and N. Koratkar , “High sensitivity detection of NO_2 and NH_3 in air using chemical vapor deposition grown graphene”, Appl. Phys. Lett. 100, 203120 (2012).
[17] S. Rumyantsev, G. Liu, M. S. Shur, R. A. Potyrailo, and A. A. Balandin, ”Selective Gas Sensing with a Single Pristine Graphene Transistor”, Nano Lett. 12, 2294−2298 (2012).
[18] C. Li, K. Fobelets, C. Liu, C. Xue, B. Cheng and Q. Wang, “Ag-assisted lateral etching of Si nanowires and its application to nanowire transfer”, Applied Physics Letters, 103(18), 183102 28 (4p) (2013).
[19] C. Panteli, O. Sydoruk, and K. Fobelets, “Suspended Graphene on Silicon Nanowire Arrays Platform for Enhanced Gas Sensing”, in preparation (2017)
20 W-K To, C-H Tsang, H-H Li, and Z. Huang, “Fabrication of n-Type Mesoporous Silicon Nanowires by One-Step Etching”, Nano Lett., 11(12), pp 5252–5258 (2011).

http://www.pdf-tools.com

[21] S. Goniszewski, J. Gallop, M. Adabi, K. Gajewski, O. Shaforost, N. Klein, A. Sierakowski, J. Chen, Y. Chen, T. Gotszalk, and L. Hao, "Self-supporting graphene films and their applications", IET Circuits, Devices and Systems 9(6), pp. 420–427 (2015).
[22] J. Yi, J. M. Lee, and W. I. Park, "Vertically aligned ZnO nanorods and graphene hybrid architectures for high-sensitive flexible gas sensors", Sensors and Actuators, B: Chemical 155 (1), pp. 264–269 (2011).
[23] Z. Ye, G. Zhang, B. Li, J. S. Strøm, G. Tong, P. J. Dahl, "Influence of airflow and liquid properties on the mass transfer coefficient of ammonia in aqueous solutions", Biosystems Eng. 100, pp. 422–434 (2008).
[24] W. Stiver and D. Mackay, "Evaporation Rate of Spills of Hydrocarbons and Petroleum Mixtures", Environ. Sci. Technol., 18, pp. 834-840 (1984).
[25] C. Li, K. Fobelets, S.N.S. Jalal, W.A. Ng, Z.A.K. Durrani, "Influence of chemical modification on the electrical properties of Si nanowire arrays", Advanced Materials Research 160-162, 1331-1335 (2011).
[26] C. Li, E. Krali, K. Fobelets, B. Cheng, and Q. Wang, "Conductance modulation of Si nanowire arrays", Appl. Phys. Lett. 101(22), 222101 (2012).
[27] C. Li, C. Zhang, K. Fobelets, J. Zheng, C. Xue, Y. Zuo, B. Cheng, and Q. Wang, "Impact of ammonia on the electrical properties of p-type Si nanowire arrays", Journal of Applied Physics 114(17), 173702 07 (2013).
[28] C. Li , B. Cheng, Q. Wang and K. Fobelets, "Conductance modulation of Si nanowire array", IUMRS-ICAM International conference on advanced materials, 22-28 Sept., Qingdao (2013) (Invited)
[29] K. Fobelets, M.M. Ahmad, S. Rumyantsev, and M.S. Shur, "Influence of ambient on conductivity and 1/f noise in Si nanowire arrays", International Conference on Noise and Fluctuations 2013*"*, 23-28 Jun Montpellier (France) (2013).
[30] K. Fobelets, M. Meghani, M.M. Ahmad, "Conductance and low frequency noise in Si nanowire arrays for gas sensing", 39th International conference on micro and nano engineering, 16-19 Sept. London, UK (2013).
[31] K. Fobelets, M. Meghani, C. Li, "Influence of Minority Carrier Gas Donors on Low Frequency Noise in Silicon Nanowires", IEEE Trans. Nanotechnol. 13(6), 1176-1180 (2014).
[32] A. A. Balandin "Low-frequency 1/*f* noise in graphene devices", Nature nanotechnology 8, pp. 549-555 (2013).

http://www.pdf-tools.com